Damage Tolerance in Hardly Coated Layer Structure with Modest Elastic Modulus Mismatch

Kee Sung Lee*
Energy Materials Research Center,
Korea Institute of Energy Research, Daejeon 305-343, Korea

A study is made on the characterization of damage tolerance by spherical indentation in hardly coated layer structure with modest elastic modulus mismatch. A hard silicon nitride is prepared for the coating material and silicon nitride with 5wt% of boron nitride composites for underlayer. Hot pressing to eliminate the effect of interface delamination during the fracture makes strong interfacial bonding. The elastic modulus mismatch between the layers is not only large enough to suppress the surface crack initiation from the coating layer but sufficiently small to prevent the initiation of radial crack from the interface. The strength degradation of the layer structure after sphere contact indentation does not significantly occur, while the degradation of silicon nitride-boron nitride composite is critical at a high load and high number of contacts.

Key Words : Layer Structure, Elastic Modulus Mismatch, Coating, Damage Tolerance, Hertzian Indentation, Spherical Indentation

1. Introduction

Silicon nitride (Si_3N_4) ceramic material can be a viable candidate for a mechanical resistant material at high temperature application (Lange, 1979). However, sometimes, boron nitride (BN) material is added for better thermal shock resistance under rapid thermal stress gradient because it has high thermal conductivity and low thermal expansion coefficient (Sinclair and Simmons, 1987; Lutz and Swain, 1992). Thus, silicon nitride-boron nitride (Si_3N_4-BN) composites can be used for nozzles, crucibles, tubes, sliding gates, and break rings. Although the BN material enhances the thermal shock resistance of ceramic materials such as Si_3N_4, microstructure observations of these composites have revealed that the additions of BN enhance microcracking and weaken the Si_3N_4/BN interface (Baskaran et al., 1993; Liu et al., 1996). Microcracking and fracture behavior along the weak interface make the composites, "machinable" and, "quasi-ductile". High machinability can have a highly adverse effect on resistance to wear and fatigue (Lee et al., 2000). For example, contact forces by rolling (Fig. 1(a)), cycling fatigue with number of cycles n (Fig. 1(b)), sliding and wear affected by normal contact force P, wave velocity ω, and velocity ν (Fig. 1(c)) as shown in Fig. 1 may cause material loss, strength degradation, and the ultimate fracture of the bearing component (Chao et al., 1995).

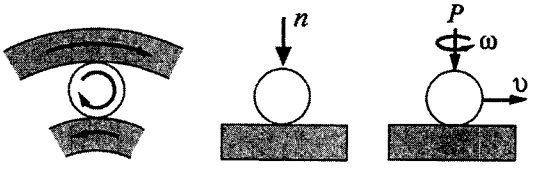

Fig. 1 Schematic diagram of the examples of contact damages on the thermal/mechanical component. (a) rolling, (b) cycling contact fatigue, and (c) sliding and wear

* **E-mail** : keeslee@kier.re.kr
TEL : +82-42-860-3414; **FAX** : +82-42-860-3133
Energy Materials Research Center, Korea Institute of Energy Research, Daejeon 305-343, Korea. (Manuscript **Received** November 11, 2002; **Revised** August 25, 2003)

Hard ceramic coatings are one of the solutions to prolong the component under wear and contact fatigue condition (Knight et al, 1989 ; Pajares et al., 1996). Hard ceramic coatings on ceramic as well as metal substrates are of great interest in relation with the protection of substrate materials and thus the flaw-insensitivity. Wear resistant coatings on the soft substrates might be potentially superior rather than substrate material itself for special combinations with both excellent wear resistance of the coatings and tougher properties of the underlayer. However, coatings or layer structures can lead to another problems such as residual stresses and mismatch of properties between layers, which can cause fracture and limit the lifetime of the component. On the other hand, mechanical and damage-resistant properties of these hard coating systems can be improved, provided the design of layer structure and material compositions are properly tailored (An et al, 1996 ; Chan et al., 1997). More recently, the effect of coating thickness and elastic modulus mismatch was investigated to demonstrate the fundamental nature of contact fracture in hard coating/soft substrate system with strong interface (Lawn et al., 2000 ; Lee, 2002).

Recent researches show that the strategy of development in high-reliability ceramics is changed to damage-insensitivity (damage tolerance) because a damage accumulation from mechanical fatigue can cause the failure of mechanical component (Suh et al., 2002 ; Lee et al., 2001). The damage tolerance can be defined as a property in which the strength of the material is not degraded by applied damage. These properties are related with the insensitivity of the strength degradation under mechanical damage (Bennison et al., 1991 ; Braun et al., 1992).

The purpose of this paper is to investigate the damage tolerance of hard Si_3N_4-coated Si_3N_4-BN composites. The top coating layer is a hard and wear resistant Si_3N_4 material. The underlayer is relatively soft and damage absorbent Si_3N_4 material with boron nitride inclusions. Only 5wt% of BN materials are added in the underlayer because our previous study showed that larger the elastic modulus mismatch between the coating and the substrate layers brings faster initiation of contact cracks (Lee, 2002). The elastic modulus mismatch between the coating layer and the underlayer is controlled as little as possible to prevent the initiation of contact-induced cracks by flexural bending of the hard coating layer (Appendix B).

Hertzian indentations are used to evaluate the damage tolerance properties (Lawn et al., 1998a ; Lawn 1998b ; Lee and Lawn, 1999). A simple contact force is applied on the surface of the material samples using hard tungsten carbide (WC) ball. The strength test after the spherical indentations is carried out for investigating the damage-insensitivity and contact fatigue resistance. The results reveal that the Si_3N_4 coating prolongs the initiation of surface flaw, and ultimately enhances the damage tolerance of the Si_3N_4-BN composites.

2. Experimental Method

2.1 Specimen preparation of hardly coated layer structure

A common powder preparation, powder stacking, and hot pressing were used for the fabrication of layer structure with strong interfacial bonding in the final product. The starting silicon nitride power mixture for the coating layer was α-Si_3N_4 (UBE-SN-E10, average particle size 0.3 μm Ube Industries America, NY) with sintering additives 5wt% Y_2O_3 (Fine Grade, H. C. Starck GmbH, Goslar, Germany), 2wt% Al_2O_3 (AKP 50, Sumitomo Chemical Co. Ltd., Tokyo, Japan), and 1wt% MgO (High Purity, Baikowski Co., N.C.). The compositions for underlayer were prepared from the same Si_3N_4 starting powder mixtures, but with 5wt% of BN (Aldrich Chemical, Milwaukee, WI, U.S.A.) additions. Each powder batch was mixed as slurry in isopropanol for 24 hr in a planetary ball mill, using zirconia (ZrO_2) balls in a polypropylene container. After drying, the softly agglomerated powder was crushed and sieved through a 60 mesh of screen. The Si_3N_4 powder mixture was stacked on Si_3N_4-BN powder mixture in the graphite mold and hot pressed to fabricate the layer structure with coat-

ing thickness 0.5 mm and substrate thickness 3 mm. Hot pressing was performed in nitrogen gas under uniaxial stress 30 MPa, at 1730℃ for 1 hr followed by furnace cooling. Hot pressing for the monolith substrate material (Si_3N_4-5wt%BN composite) was also performed at the same sintering condition for comparison in this study.

Surface of each specimen was ground, cut into 3 mm×4 mm×25 mm bars, and polished to 1 μm finish to enable characterization and indentation testing. Coating thickness was controlled in the range of $d=100\pm20$ μm by mechanical grinding and polishing. The side surfaces including the interface between two layers were plasma etched to reveal the microstructure by scanning electron microscopy (SEM). The sintered density was measured by Archimedes principle.

2.2 Mechanical characterization

Vickers indentation tests were made on each layer monolith at load $P=100$ N. Hardness, H and toughness, T_o were measured using following equations.

$$H=P/2a^2 \tag{1}$$

where, P is indentation load, and a is average value of half-diagonal lengths.

$$T_o=\chi P/c^{3/2} \tag{2}$$

where, $\chi=0.016(E/H)^{1/2}$ with elastic modulus E and hardness H, and indentation crack length c.

Simple spherical indentation was made on the polished surfaces of each layer monolith to evaluate elastic modulus E, yield stress Y, and strain hardening coefficient α by the indentation stress-strain curve described in our previous study (Lee, 2002). The indentations were made at loads up to $P=4000$ N to measure the sizes of damages on each specimen using universal testing machine (Model 1122, Instron Corp.).

The opposing surfaces of two same specimens were polished and glued together, with glue thickness $t\leq10$ μm, to produce, "bonded-interface" specimens for investigation of subsurface damage in spherical contact tests (Guiberteau, 1994). The indentations were made on the top surfaces using WC spheres with a radius of $r=1.98$ mm at load $P=2000$ N. After indentation, the bonded-interface specimens were soaked in acetone to dissolve the adhesive and separate the specimens into two. After cleaning the surfaces, the side surfaces were gold-coated and viewed in optical Nomarski illumination.

Damage tolerances were carried out on the Si_3N_4 coating system (Si_3N_4-coated Si_3N_4-5wt% BN composite) and the substrate material (Si_3N_4-5wt%BN composites) by flexural bending test after Hertzian indentation in the universal testing machine. Figure 2(a) shows the schematic diagram of spherical indentation on the specimen and continuous strength tests. Bar specimens were indented in air at the center of polished face using

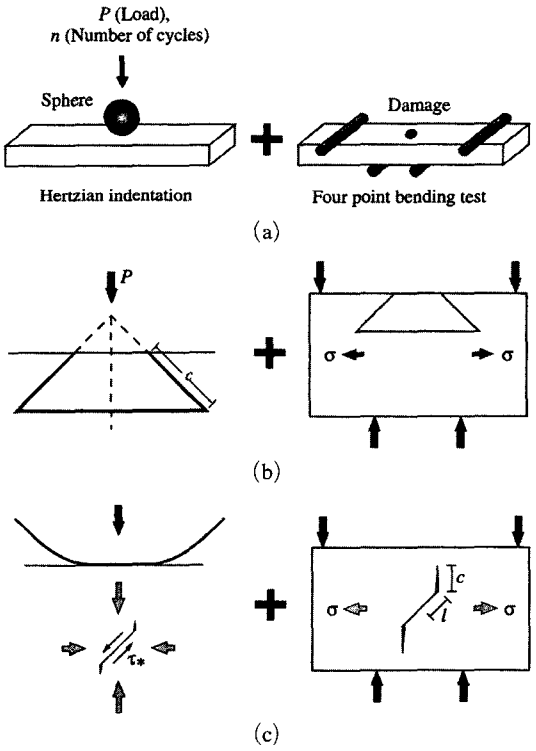

Fig. 2 Schematic diagram of damage tolerance test against damages produced by spherical indentation ; (a) experimental set up, (b) damage tolerance test on the material that included cone crack, and (c) damage tolerance test on the material that included microcracks on shear fault

WC ball with a radius of 1.98 mm at contact loads from $P=1000$ N to 4000 N by universal testing machine (Model 1122, Instron Corp.). The other multi-cycle contact tests were performed at load $P=1000$ N over 10^6 cycles at a frequency of 10 Hz (Model 8502, Instron Corp.) Typical examples of contact-induced damages are tensile-driven, "cone cracks" from the surface immediately outside the contact as shown in Fig. 2(b) and shear-driven, "quasi-plastic yield zone" containing microcracks below the contact in Fig. 2(c) (Lawn, 1998b). Indented specimens were broken in flexure with the polished sides in tension with a crosshead speed of 30 mm/min, using four-point support on a universal test machine. The strengths were calculated from beam theory, using the conventional relation

$$\sigma_F=3Fl/4wd^2 \tag{3}$$

with l the moment span, w the bar width, d the sample thickness and F the breaking load. The bending tests follow the extension of contact damages by tensional stresses, σ. The fracture strength contained the contact cracks in the surface depends on the crack length c in Eq. (4) (Lawn, 1998a).

$$\sigma_F=T_o/\psi c^{1/2} \tag{4}$$

where ψ is the geometrical coefficient.

On the other hand, the damages produced by critical shear stress, τ^*, in the quasi-plastic ceramics affects the strength in Eq. (5).

$$\sigma_F=(3/4\psi)\,[T_0^4/4\chi\lambda l^2\tau^*]^{1/3} \tag{5}$$

where l microstructural fault radius and $\lambda=Q/l^2\tau^*$ with Q, center-loaded force on pennylike crack.

Surfaces of indented specimens were sputter-coated with gold and viewed in an optical microscope (Nomarski illumination). Some specimens were prepared without spherical indentations, for measurement of, "laboratory" strengths. All broken specimens were also examined by optical microscopy in Nomarski illumination to confirm the failure origin.

3. Results and Discussion

In this study we represent the damage tolerance of Si_3N_4 coated Si_3N_4-5wt%BN composite relative to that of Si_3N_4-5wt%BN composite. We select the 5wt%BN composition from taking into account the influence of elastic modulus mismatch on indentation stresses evaluated from fracture mechanics consideration (Appendix A) and maximum tensile stresses evaluated from FEM analysis (Appendix B).

The result of SEM examination on the Si_3N_4 coated Si_3N_4-5wt%BN composite is shown in Fig. 3. The microstructure revealed that relatively isotropic in the Si_3N_4 coating layer and highly anisotropic in the Si_3N_4-BN substrate layer. The microstructures of the coating layer and the matrix material in the underlayer are similar to each other, irrespective of the coating and the substrate layer. They have elongated grains of length ~ 3 μm and diameter ~ 0.8 μm. The examination also shows the BN as a platelet in the underlayer. The large elongated remnant voids in the material correspond to the BN platelets, dislodged during plasma etching (Liu et al., 1996). The BN has the form of platelets 1.5~6 μm diameter and 0.2~0.6 μm thickness, with these platelets strongly aligned normal to the hot pressing direction, which is parallel to the coating/substrate interfaces.

Indentation stress-strain curves for the Si_3N_4 coating material and the Si_3N_4-5wt%BN substrate monolith are shown in Fig. 4. The curves show nonlinearity in the stress-strain curve above the

Fig. 3 SEM micrograph of Si_3N_4 coated Si_3N_4-5wt%BN composite

yield point. As the BN is added in the Si_3N_4, the curve is slightly deviated from that of the Si_3N_4 coating material. The solid curve fit of the Si_3N_4-5wt%BN material shows a shift away from that of the hard Si_3N_4 coating material, indicating softer characteristics of the substrate material in this study. The role of the soft substrate in determining the stress-bearing capacity will be manifest when we make the layer structure using these materials. The deviation of two curves is not too large comparing to the indentation stress-strain curve of Si_3N_4-30wt%BN material in our prior study (Lee, 2002). Thus, the Si_3N_4 coated Si_3N_4-5wt%BN composite is a layer structure with modest elastic modulus mismatch between the coating and the substrate layer.

The characteristics of individual layer materials were summarized in Table 1. Hardness and toughness are calculated from equations (1) and (2) after Vickers indentation on the flat polished surfaces. While the hardness of Si_3N_4 is relatively high, the fracture toughness of Si_3N_4-5wt%BN composite shows higher value. The Si_3N_4-5wt% BN composite has a relatively higher toughness because of microcracking and crack deflection along the weak interface. Elastic modulus, yield stress, and strain hardening coefficient of each individual layer materials are from the indentation stress-strain data of Fig. 4. The elastic modulus, yield stress, and straining hardening coefficient of each material is calculated from a similar way with our prior analysis (Lee, 2002), and represented in the Table 1. Thus, the elastic modulus mismatch and plastic mismatch, E_c/E_s, Y_c/Y_s, α_c/α_s are maintained in the range of 1.0~1.4. Therefore a hardly coated layer structure with modest elastic modulus mismatch is prepared in this study. This layer structure has strong interfacial bonding without possessing influential residual stresses in any layer (Lee, 2002; Song et al., 2002; Lee, 1997).

Table 1 Characteristics of Si_3N_4 and Si_3N_4-5wt%BN composite

Characteristics	Si_3N_4	Si_3N_4-5wt%BN
Relative density (%)	>99	>99
Hardness, H(GPa)	14.6±0.5	12.6±0.6
Toughness, T_o(MPam$^{1/2}$)	5.7±0.5	7.8±0.9
Elastic modulus, E(GPa)	320.0±64.0	278.0±56.0
Yield stress, Y(GPa)	8.4±015	6.7±0.21
Strain hardening coefficient	0.7±0.05	0.5±0.05

Half-surface section views of the contact damage indented by WC spheres, $r=1.98$ mm at a

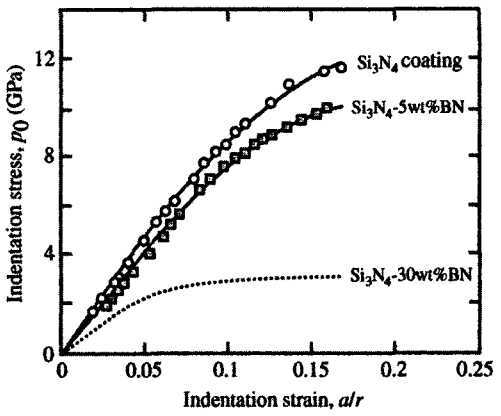

Fig. 4 Indentation stress-strain curves for each layer material used in the coating (Si_3N_4) and the substrate (Si_3N_4-5wt%BN). A curve for the Si_3N_4-30wt%BN material is included in the graph

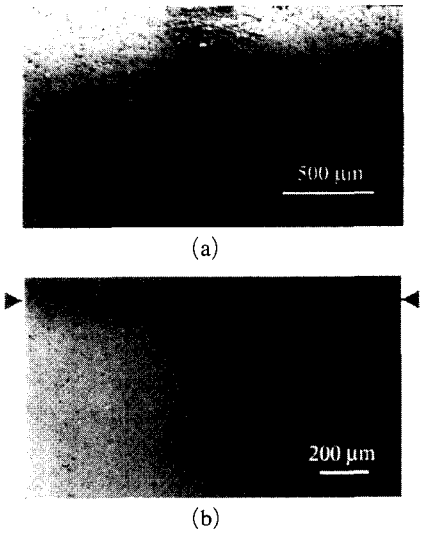

Fig. 5 Contact damages in (a) Si_3N_4-5wt%BN composite and (b) Si_3N_4 coated Si_3N_4-5wt%BN composite, after spherical indentation with WC sphere radius $r=1.98$ mm at load $P=2000$ N. Arrows indicate the interlayer interface region

load of P=2000 N are shown in Fig. 5. In the Si_3N_4-5wt%BN composite, extended subsurface damage is apparent by shear stress. The cone crack is not detected beneath the contact site, because the quasi-plastic characteristic of the substrate material produces an extensive yield zone instead of cone-shaped cracks by tensile stress under the contact load. The micrograph in Fig. 5(a) shows microcracks and their some coalescence in the subsurface damage zone. On the other hand, quasi-plastic yield zone did not observed in the coating layer for the Si_3N_4 coated Si_3N_4-5wt%BN composite. Cone cracks never appear in most cases at the same stress. However, instead of subsurface damage, a small crack is sometimes observed under the coating layer (Fig. 5(b)). Consequently, hard Si_3N_4 coating layer protects the Si_3N_4-BN composites from the formation of surface damage.

Serial surface views of contact damage in the Si_3N_4-5wt%BN composite under the contact load from P=1000 N to P=4000 N are shown in Fig. 6. Surface damages are apparent in this composite material. A surface impression ("quasi-plastic" mode) is already evident at P=1000 N, and the size of impressions increases according to the increasing load from P=2000 N to P=3000 N. It is described in prior study that this kind of damage of heterogeneous structure manifests as a cloud of closed shear microcracks or shear faults within a shear-compression deformation zone above critical point under the critical load (Lee et al., 2000). With further loading to P=4000 N, the largest damage zone with the radial cracks are shown. The radial cracks accelerated by coalescence of adjacent faults under extreme contact conditions have been described in our prior results (Lee et al., 2000).

In the Si_3N_4 coated Si_3N_4-5wt%BN composite, the production of the apparent surface damages caused by shear stresses was suppressed as shown in Fig. 7. Any surface damages could not be found on the surface of the coating layer up to P=2000 N, and slight surface compression is observed at P=3000 N caused by the influence of softer substrate. Finally cone crack pop-in abruptly in the coating layer at P=4000 N because this contact condition is beyond the load of cone crack initiation of Si_3N_4 monolith, P_c= 2000±200 N. Note the radial crack does not appear at P=4000 N in this composite. It is also noteworthy that the cone crack did not appear at P=3000 N, which is beyond the critical load of crack initiation for the Si_3N_4 coating monolith. It is thought that softer substrate can offer damage tolerance by redistributing the tensile stresses

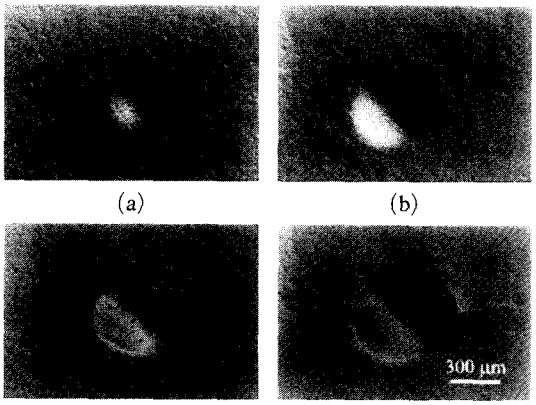

Fig. 6 Micrographs of surface damage in Si_3N_4-5wt %BN composite from spherical indentation with WC sphere radius r=1.98 mm at load (a) P=1000 N, (b) P=2000 N, (c) P= 3000 N, and (d) P=4000 N

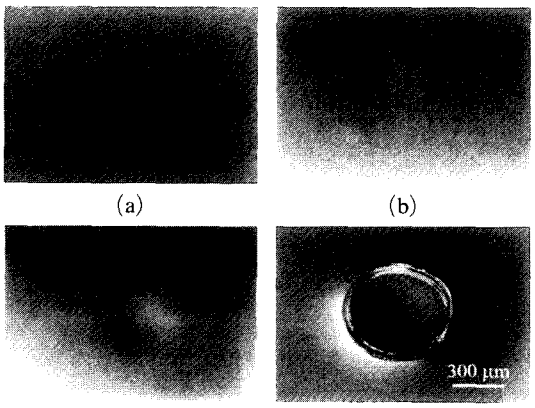

Fig. 7 Micrographs of surface damage in Si_3N_4 coated Si_3N_4-5wt%BN composite from spherical indentation with WC sphere radius r= 1.98 mm at load (a) P=1000 N, (b) P= 2000 N, (c) P=3000 N, and (d) P=4000 N

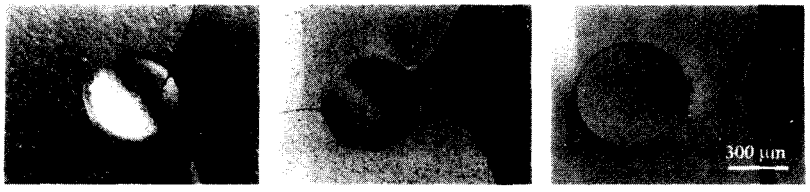

(a) (b) (c)

Fig. 8 Surface views of contact failure sites after spherical indentation with WC sphere radius $r=1.98$ mm at load (a) $P=3000$ N in Si_3N_4-5wt%BN composite, (b) $P=4000$ N in the Si_3N_4-5wt%BN composite, and (c) $P=4000$ N in Si_3N_4 coated Si_3N_4-5wt%BN composite

(Chai, 1999).

Figure 8 shows the representative fracture origins produced the Si_3N_4 coated Si_3N_4-5wt%BN composite or the Si_3N_4-5wt%BN composite. The figure shows failure origins on broken strength test specimens containing indentations from WC spheres of radius $r=1.98$ mm, (a) in the Si_3N_4-5wt%BN composites, at $P=3000$ N (b) in the Si_3N_4-5wt%BN composites, at $P=4000$ N, and (c) in the Si_3N_4 coated Si_3N_4-5wt%BN composite, at $P=4000$ N. Failure modes are indicated by peripheral fracture paths tangent to the damages. Fracture paths in the Si_3N_4-5wt%BN composite at $P=3000$ N pass through the yield zone. This phenomenon indicates that fracture originated from the flaw in the subsurface damage zone. The fracture paths at higher load, $P=4000$ N, moves to the radial cracks rather than the yield zone. On the other hand, the fracture paths in the Si_3N_4 coated Si_3N_4-5wt%BN composite come from cone cracks as shown in Fig. 8(c). All micrographs confirm that all failures are started from the surface damages formed by spherical indentation.

Data for the strengths σ_F from Fig. 2 and eq. (3) in the Si_3N_4 coated Si_3N_4-5wt%BN composite or the Si_3N_4-5wt%BN composite are plotted as a function of contact load P in Fig. 9. Boxes at left axis denote, "laboratory" or, "inert" strengths of unindented specimens. Open symbols indicate the strength data of the Si_3N_4-5wt%BN composite. Dark symbols for the Si_3N_4 coated Si_3N_4-5wt% BN composite. While the Si_3N_4-5wt%BN composite loses its inert strength from $P=2000$ N, the Si_3N_4 coated Si_3N_4-5wt%BN composite relatively do not reduce the strength until $P=4000$ N. The

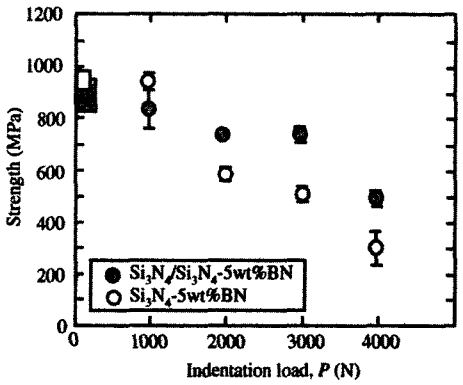

Fig. 9 Strength degradations of Si_3N_4-5wt%BN composite and Si_3N_4 coated Si_3N_4-5wt%BN composite after spherical indentation. Shaded boxes at left axis represent strengths of unindented specimens

strength of the Si_3N_4-5wt%BN composite reduces at $P=2000$ N due to microcrack coalescence (Fig. 5(a)), and fall down very much (almost less than half-value of initial strength) at $P=4000$ N because of radial crack produced on the surface (Fig. 6(d)). The radial cracks are ultimate result of the coalescence of microcracks under contact fatigue. It was suggested that the spherical indenters ultimately penetrates in the quasi-plastic ceramics at highest damage and behave as, "sharp" indenters (Lee et al., 2000). The Si_3N_4 coating prevents the evolution of this critical radial cracks. Therefore the damage tolerance of the Si_3N_4 coated Si_3N_4-5wt%BN composite at highest load is closely related with the prevention of surface flaw production.

Inert strengths σ_F as a function of number of cycles, n, at $f=10$ Hz, indentation with WC spheres at maximum load $P=1000$ N on two

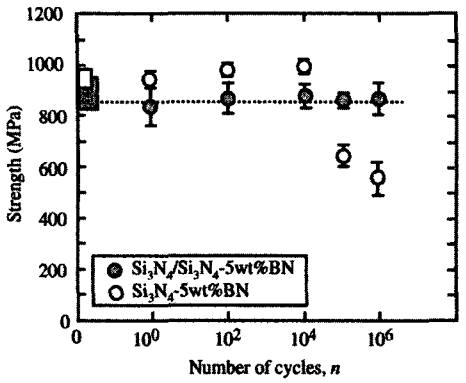

Fig. 10 Strengths of Si_3N_4-5wt%BN composite and Si_3N_4 coated Si_3N_4-5wt%BN composite as a function of number of cycles after spherical indentation in air with WC sphere radius $r=1.98$ mm at load $P=1000$ N and frequency $f=10$ Hz. Shaded boxes at left axis represent breaks from specimens without indentations

materials are plotted in Fig. 10. The loads chosen are sufficient to produce failures from indentation origins as a thermal/mechanical component in all cases. The strength losses are strongly enhanced at certain number of cycles in the Si_3N_4-5wt%BN composite relative to the Si_3N_4 coated Si_3N_4-5wt%BN composite. In comparison to specimens without indentations (box at left axis), the strength of the Si_3N_4-5wt%BN composite is maintained the initial strength until $n=10^4$ and fall down from $n=10^5$. On the other hand, the strength of the Si_3N_4 coated Si_3N_4-5wt%BN composite is not degraded until $n=10^6$. Therefore the damage tolerance of the Si_3N_4 coated Si_3N_4-5wt% BN composite is much clearer basing on this result. The Si_3N_4 coated Si_3N_4-5wt%BN composite has a markedly reduced sensitivity to indentation load with high number of cycles, i.e. has a greater, "damage tolerance". Therefore the lifetime of the Si_3N_4 coated Si_3N_4-5wt%BN composite can be improved from the hard coating on soft substrates.

In this study the importance of layer structure design is addressed. Our study showed that larger elastic modulus mismatch (larger E_c/E_s, smaller E_s/E_c) between the coating and the substrate layer caused faster crack initiation (Appendix B). When the crack happens in the brittle ceramic material at surface or subsurface, it will cause severe strength degradation (Lawn, 2000). Therefore designing a layer structure with modest elastic modulus mismatch is important to prevent the strength degradation under the damage. Our study suggests a meaningful design by layered structure, especially against crack initiation rather than crack propagation in the brittle material such as ceramics because one single crack is an ultimate cause of failure if it occurs catastrophically, deflected, or bridged.

Over the last decade there has been a lot of works to enhance the fracture toughness and fatigue properties against crack propagation by microstructure control or making composites (Lawn, 1993). However it is reported that the susceptibility of tough ceramics to fatigue is pronounced in cyclic contact loading with hard spheres (Lee et al., 2000). On the other hand, this study shows the crack initiation can be delayed by layered design with maintaining modest elastic modulus mismatch, $E_c/E_s=1.15/1$ and coating thickness, $d_c/d_s=1/30$, and ultimately the damage tolerance can be obtained against contact crack initiation.

4. Conclusion

(1) In this study, we investigated the damage tolerance of the Si_3N_4 coated Si_3N_4-5wt%BN composite with modest elastic modulus mismatch, $E_c/E_s=1.15/1$. Thick Si_3N_4 hard coating was performed ; $d_c=100\pm20$ μm. We have used spherical indentations to demonstrate the surface damage mode and investigated strength degradation.

(2) The surface damage was suppressed by hard coating, and ultimately the strength degradation was delayed. The formation of critical surface damage was also delayed in the Si_3N_4 coated Si_3N_4-5wt%BN composite compared to the Si_3N_4-5wt%BN composite.

(3) The result of this study indicates that Si_3N_4-coated layer structure is more damage tolerant if the design of layer structures is modestly tailored.

APPENDIX A

Indentation Stresses in the Si_3N_4-coated layer structure

In this appendix, we consider indentation stresses to cause a local material deformation in the Si_3N_4-coated layered composite. Consider the contact (load P) of a coating system with coating thickness d, using a sphere with a radius r as depicted in Fig. A1. Two factors distinguish the coating system from the bulk structure, first, a coating thickness, d, in relation to the sphere radius r, and secondly, a material factor E_s/E_c representing substrate/coating elastic modulus mismatch.

We use simple empirical formulation by Hu (Hu and Lawn, 1998), for bilayer systems. According to the formulation we write the indentation stress,

$$p_0=(4E_{cs}'/3\pi)(a/r) \quad \text{(A1)}$$

where E_{cs}' is a composite modulus given by

$$E_{cs}'=E_c'(E_s'/E_c')^L \quad \text{(A2)}$$

with $L=L(a/d)$ a geometry term. We can rewrite eq. (1) in normalized form

$$p_o/E_{cs}'=(4/3\pi)(E_s'/E_c')^{L(a/d)}(a/r) \quad \text{(A3)}$$

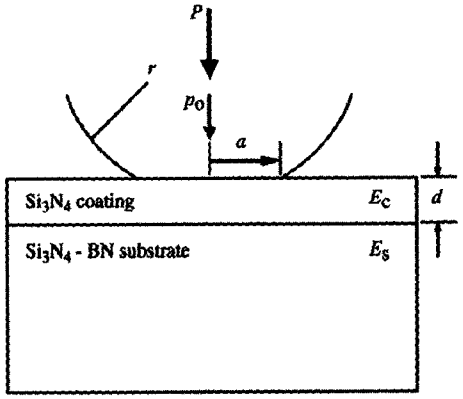

Fig. A1 Contact of a sphere on a coating/substrate layer composite showing key indentation variables

An empirical determination of $L(a/d)$ gives (Hu and Lawn, 1998)

$$L(a/d)=1-\exp\{-[A+B\ln(a/d)]^M\} \quad \text{(A4)}$$

with $A=0.749$, $B=0.173$ and $M=4.72$.

Therefore we can plot p_o/E_c' as a function of E_s/E_c at fixed a/d, or as a function of d at fixed E_s/E_c for the fixed value of contact radius a as shown in Fig. A2 and Fig. A3. The dotted line in the Fig. A2 denotes the elastic modulus mismatch of the Si_3N_4 coated Si_3N_4-5wt%BN composites. Figure A2 indicates that the increase of E_s/E_c is beneficial to increase the indentation stresses to cause a surface deformation, which is closely related with higher strength. The composite with modest elastic modulus mismatch (5BN) shows that the indentation stress is not sensitive to the coating thickness as shown in Fig. A3.

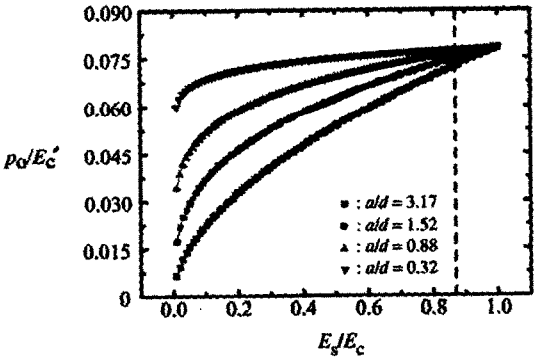

Fig. A2 Plot of p_o/E_c' of bilayer composite as a function of E_s/E_c, for variable a/d

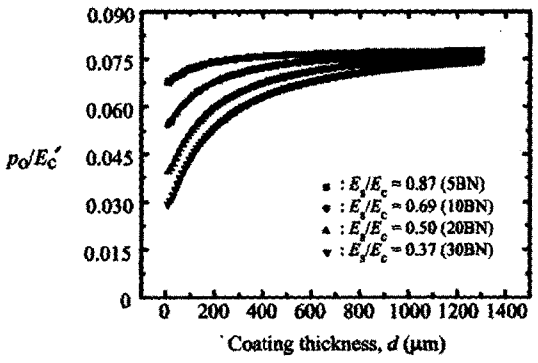

Fig. A3 Plot of p_o/E_c' of bilayer composite as a function of coating thickness, d

APPENDIX B

FEM Analysis on the Si_3N_4 coated Si_3N_4-BN composites with different amounts of BN contents

Finite element modeling (FEM) of stresses during the contact tests was carried out using a commercial package (Strand, G&D Computing, Sydney, Australia) for generating the data in Fig. B1. The algorithm consists of a sphere of specified radius in axisymmetric frictionless contact on the flat coating layers. Strong interfacial bonding is assumed. For the bilayer structures, each material layer is allowed to yield according to a critical shear stress condition, in conjunction with a bilinear uniaxial stress-strain function $\sigma(\varepsilon)$ (Fischer-Cripps et al., 1996)

$$\sigma = E\varepsilon \qquad (\sigma \leq Y) \qquad \text{(B1)}$$

$$\sigma = Y + \alpha(\varepsilon E - Y) \qquad (\sigma \geq Y) \qquad \text{(B2)}$$

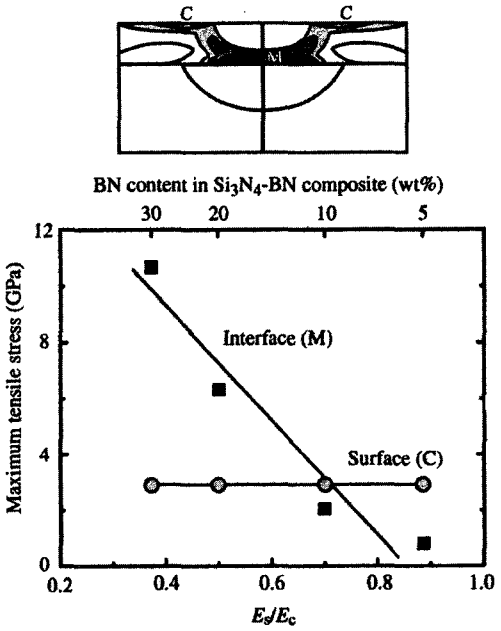

Fig. B1 Plot of maximum tensile stress and the stress contour versus E_s/E_c for Si_3N_4 on Si_3N_4-BN with coating thickness $d=250$ μm, using WC sphere $r=1.98$ mm at $P=2000$ N. Maximum principal tensile stresses were calculated in the interface and surface regions during the contact test

with α a dimensionless strain-hardening coefficient in the range $0 \leq \alpha \leq 1$ ($\alpha=1$, fully elastic; $\alpha=0$, fully plastic).

The maximum stress was calculated from corresponding point-by-point computations of the principal stresses below the contact. The maximum tensile stress in the FEM-generated contour was calculated from each data of elastic modulus, E, yield stresses, Y, and strain hardening coefficients, α, of Si_3N_4-BN composites with different amount of BN content (Lee, 2002), using WC sphere $r=1.98$ mm at $P=2000$ N.

Typical FEM-generated contours of principal stresses in the Si_3N_4 coated Si_3N_4-BN composite are shown in Fig. B1. Principal stresses at shaded areas correspond to tensile zones ($\sigma_1 \geq 0$) and white areas indicate compressive zones. The initiation of cracks is started from the region of the highest tensile stress just above the interface (M) between the coating and the substrate layer, or the region of the highest tensile stress immediately outside the contact circle (C). Figure B1 shows the maximum tensile stress as a function of elastic modulus mismatch, E_s/E_c, for the Si_3N_4 coated Si_3N_4-BN composite with coating thickness $d=250$ μm at load $P=2000$ N. The interface stress maximum is highly sensitive to the BN content relative to the surface maximum stress. The result of Fig. B1 indicates that the Si_3N_4 coated Si_3N_4-5wt%BN composite is an appropriate hardly coated layer composite with modest elastic modulus mismatch, that is, it does not cause a transverse crack, which is initiated from the interface stress maximum caused by the mismatch of elastic modulus between the coating and the substrate layer in the layer structure with higher amount of BN.

Acknowledgment

I am grateful to Dr. Brian Lawn in NIST, USA and Dr. Do Kyung Kim in KAIST, Korea for their helpful discussion and advice.

References

An, L., Chan, H. M., Padture, N. P. and Lawn, B. R., 1996, "Damage-Resistant Alumina-Based

Layer Composites," *Journal of Materials Research*, Vol. 11, No. 1, pp. 204~210.

Baskaran, S., Nunn, S. D., Popovic, D. and Halloran, J. W., 1993, "Fibrous Monolithic Ceramics : I. Fabrication, Microstructure, and Indentation Behavior," *Journal of the American Ceramic Society*, Vol. 76, No. 9, pp. 2209~2216.

Bennison, S. J., Padture, N. P., Runyan, J. L. and Lawn, B. R., 1991, "Flaw-Insensitive Ceramics," *Philosophical Magazine Letters*, Vol. 64, pp. 191~195.

Braun, L. M., Bennison, S. J. and Lawn, B. R., 1992, "Short-Crack T-Curves and Damage Tolerance in Alumina-Based Composites," *Composites and Advanced Ceramic Materials*, Vol. 13, pp. 156~163.

Chai, H., Lawn, B. R. and Wuttiphan, S., 1999, "Fracture Modes in Brittle Coating with Large Interlayer Modulus Mismatch," *Journal of Material Research*, Vol. 14, pp. 3805~3817.

Chan, H. M., 1997, "Layered Ceramics : Processing and Mechanical Behavior," *Annual Review of Materials Research*, Vol. 27, pp. 249~282.

Chao, L. Y., Lakshminarayanan, R., Shetty, D. K. and Culter, R. A., 1995, "Rolling-Contact Fatigue and Wear of CVD-SiC with Residual Surface Compression," *Journal of the American Ceramic Society*, Vol. 78, No. 9, pp. 2307~2313.

Fischer-Cripps, A. C. and Lawn, B. R., 1996, "Stress Analysis of Contact Deformation in Quasi-Plastic Ceramics," *Journal of the American Ceramic Society*, Vol. 79, No. 10, pp. 2609~2618.

Guiberteau, F., Padture, N. P. and Lawn, B. R., "Effect of Grain Size on Hertzian Contact Damage in Alumina," *Journal of the American Ceramic Society*, Vol. 77, No. 7, pp. 1825~1831.

Hu, X. Z. and Lawn, B. R., 1998, "A Simple Indentation Stress-Strain Relation for Contacts with Spheres on Bilayer Structures," *Thin Solid Films*, Vol. 322, Issues 1-2, pp. 225~232.

Knight, J. C., Page, T. F. and Hutchings, I. M., 1989, "The Influence of Substrate Hardness on the Response of TiN-Coated Steels to Surface Deformation," *Thin Solid Films*, Vol. 177, pp. 117~132.

Lange, F. F., 1979, "Fracture Toughness of Si_3N_4 as a Function of the Initial α-Phase Content," *Journal of the American Ceramic Society*, Vol. 62, No. 7-8, pp. 428~430.

Lawn, B. R., 1993, Fracture of Brittle Solids, Cambridge University Press, Cambridge, U.K.

Lawn, B. R., Lee, S. K., Peterson, I. M., Wuttiphan, S., 1998a, "A Model of Strength Degradation from Hertzian Contact Damage in Tough Ceramics," *Journal of the American Ceramic Society*, Vol. 81, No. 6, pp. 1509~1520.

Lawn, B. R., 1998b, "Indentation of Ceramic with Spheres : A Century After Hertz," *Journal of the American Ceramic Society*, Vol. 81, No. 8, pp. 1977~1994.

Lawn, B. R., Lee, K. S., Chai, H., Pajares, A., Kim, D. K., Wuttiphan S., Peterson I. M. and Hu Xiaozhi, 2000, "Damage-Resistant Brittle Coatings," *Advanced Engineering Materials*, Vol. 11, pp. 745~748.

Lee, O. S., 1997, "Residual Stress Interference by Two Micro-Vickers Indentation," *KSME International Journal*, Vol. 11, No. 4, pp. 379~385.

Lee, K. S., Jung, Y. G., Peterson, I. M., Lawn, B. R., Kim, D. K. and Lee, S. K., 2000, "Model for Cyclic Fatigue of Quasi-Plastic Ceramics in Contact with Spheres," *Journal of the American Ceramic Society*, Vol. 83, No. 9, pp. 2255~2262.

Lee, K. S., 2002, "Effect of Elastic Modulus Mismatch on the Contact Crack Initiation in Hard Ceramic Coating Layer," *KSME International Journal*, accepted.

Lee, K. Y., Choi S. J. and Youn J. W., 2001, "Surface Damage Accumulation in Alumina under the Repeated Normal Tangential Contact Forces," *KSME International Journal*, Vol. 1, pp. 48~51.

Lee, S. K. and Lawn, B. R., 1999, "Contact Fatigue in Silicon Nitride," *Journal of the American Ceramic Society*, Vol. 82, No. 5, pp. 1281~1288.

Liu, H., Lawn, B. R. and Hsu, S. M., 1996, "Hertzian Contact Response of Tailored Silicon Nitride Multilayers," *Journal of the American Ceramic Society*, Vol. 79, No. 4, pp. 1009~1014.

Lutz, E. H. and Swain, M. V., 1992, "Fracture

Toughness and Thermal Shock Behavior of Silicon Nitride-Boron Nitride Ceramics," *Journal of the American Ceramic Society*, Vol. 75, No. 1, pp. 67~70.

Pajares, A., Wei, L., Lawn, B. R. and Berndt, C. C., 1996, "Contact Damage in Alumina-Based Plasma Sprayed Coatings," *Materials Science and Engineering*, Vol. A208, No. 2, pp. 158~165.

Sinclair, W. and Simmons, H., 1987, "Microstructure and Thermal Shock Behavior of Composites," *Journal of Materials Science Letters*, Vol. 6, pp. 627~629.

Song, J. H., Kim, H. K. and Lim, J. K., 2002, "Evaluation of Apparent Interface Toughness of Composites Layers by Indentation Test," *Transaction of KSME*, Vol. 26, No. 10, pp. 2089~2095.

Suh, C. M., Hwang B. W. and Murakami R. I., 2002, "Characteristics of Fatigue Crack Initiation and Fatigue Strength of Nitrided 1Cr-1Mo-0.25V Turbine Rotor Steels," *KSME International Journal*, Vol. 16, pp. 1109~1116.